COMMUNICATION

Local surface structure and composition control the hydrogen evolution reaction on iron nickel sulfides

Cameron L. Bentley,‡[a] Corina Andronescu,‡[b,c] Mathias Smialkowski,‡[d] Minkyung Kang,[a] Tsvetan Tarnev,[b] Bernd Marler,[e] Patrick R. Unwin,*[a] Ulf-Peter Apfel,*[d] Wolfgang Schuhmann*[b]

Abstract: In order to design more powerful electrocatalysts, developing understanding of the role of surface atomic-structural composition of widely abundant bulk materials is crucial. This is particularly true in the search for alternative hydrogen evolution reaction (HER) catalysts that can replace platinum. We report scanning electrochemical cell microscopy (SECCM) measurements of the (111)-crystal planes of $Fe_{4.5}Ni_{4.5}S_8$, a highly active HER catalyst. In combination with structural characterization methods, we show that this technique can reveal differences in activity arising from even the slightest compositional changes. By probing electrochemical properties at the nanoscale level, in conjunction with complementary atomic/structural information, novel design principles emerge to be applied for rational material synthesis.

In recent years, hydrogen (H_2) has attracted increasing attention for energy storage and utilization.[1,2] While it is currently generated predominantly from fossil fuels,[3–5] water splitting by electrocatalysis is the desired method for sustainably generating H_2, as this would enable energy storage from various renewable sources.[6] Among the most active electrocatalysts for the hydrogen evolution reaction (HER) is platinum and its alloys,[7] which are expensive, rare and require the use of non-corrosive (non-poisoning) electrolyte solutions.[8] For these reasons, there has been a drive to develop alternative (electro)catalysts, such as metal chalcogenides,[9–13] which have been shown to efficiently catalyze the HER, sustaining high current densities at relatively low overpotentials.[1,5,14,15]

We recently reported on highly conductive $Fe_{4.5}Ni_{4.5}S_8$ as an efficient HER catalyst that is able to operate under otherwise "poisoning" conditions.[16,17] Notably, in its bulk form (*i.e.*, without any need for elaborate nanoparticle preparation), this iron nickel sulfide achieved a current density (J) of 10 mA cm^{-2} at an overpotential (η) of as low as 190 mV for surface activated samples (280 mV for the as synthesized material) and further sustained a catalytic rate of 2.14 mmol H_2 h^{-1} cm^{-2} for more than 170 h at high J (> 600 mA cm^{-2}). Operando phonon studies on this material also showed that upon long-term electrolysis, surface sulfur is replaced by protons, leading to the formation of a highly reactive FeNi-hydride surface.[18] Furthermore, it was shown electrochemically that while non-uniform Fe/Ni distributions on the electrode surface produced no notable alteration of the bulk electrocatalytic performance in the freshly synthesized material, long-term electrolysis (*i.e.*, days timescale) led to a decreased HER activity at disparate Fe/Ni ratios. These observations suggest that the atomic surface composition is more important for high catalytic activity than nanostructuring in this class of material.

Electrocatalytic investigations are usually performed with macroscopic voltammetric techniques to reveal the "average" properties of a bulk material (as in $Fe_{4.5}Ni_{4.5}S_8$) or nanoparticle ensemble. By contrast, scanning electrochemical cell microscopy (SECCM), a high resolution electrochemical imaging technique, is able to directly probe catalytic activity at the nanoscale by targeting characteristic surface sites, and, when combined with information from other imaging and spectroscopic techniques, allows structure to be unequivocally related to function, an omnipresent goal in materials science.[19–23] Indeed, the power of this technique was recently highlighted for the HER catalyst molybdenum disulfide (MoS_2)[8,24], where moderate (albeit, much higher than previously reported[15,25,26]) and high catalytic activity was *measured directly at the basal and edge planes*, respectively. Such an approach aims to identify the structural features which constitute an active surface (*e.g.*, edge plane of MoS_2) at the micro-/nanoscale, which can guide catalyst design and synthesis at the macroscale. In order to obtain an in-depth correlation between structural parameters (*i.e.*, exposed crystallographic facet and/or atomic composition) and the electrochemical properties (*e.g.*, catalytic activity) of the complex bimetallic HER catalyst, $Fe_{4.5}Ni_{4.5}S_8$, we report spatially-resolved SECCM studies performed on the bulk crystalline material, where the location of the measurement can be determined.

Bulk $Fe_{4.5}Ni_{4.5}S_8$ was synthesized following our previously reported procedure starting from the constituent elements in sealed quartz ampules.[16,17] Subsequent high temperature treatment at 860°C of finely grounded $Fe_{4.5}Ni_{4.5}S_8$ containing 26 % iodine afforded two sets of different crystals over a period of 16 days (Figure 1A and B). Both the platelets (Figure 1A) and hexagonal crystals (Figure 1B), reveal the same powder X-ray diffraction patterns showing the same overall crystallographic structure (Supporting Information, Figure S1). In addition, electron backscatter (EBSD) diffraction patterns suggest the preferential formation of (111)-surfaces (Supporting Information, Figure S2). The connectivity of the elements was further verified by single crystal X-ray analysis on the hexagonal crystals (Figure 1C) and

[a] Dr. C. L. Bentley, Dr. M. Kang, Prof. Dr. P. R. Unwin
Department of Chemistry; University of Warwick
Coventry CV4 7AL (U.K.)
E-mail: P.R.Unwin@warwick.ac
[b] Dr. C. Andronescu, T. Tarnev, Prof. Dr. W. Schuhmann
Analytical Chemistry - Center for Electrochemical Sciences (CES)
Ruhr-Universität Bochum; Universitätsstrasse 150,
D-44780 Bochum (Germany)
E-mail: wolfgang.schuhmann@rub.de
[c] Dr. C. Andronescu
University Politehnica of Bucharest, Department of Bioresources and Polymer Science, 1-7 Gh. Polizu Street, Bucharest (Romania)
[d] M. Smialkowski, Dr. U.-P. Apfel
Inorganic Chemistry I: Ruhr-Universität Bochum
Universitätsstrasse 150, D-44780 Bochum (Germany)
E-mail: ulf.apfel@rub.de
[e] Dr. B. Marler; Department of Geology, Mineralogy and Geophysics
Ruhr-Universität Bochum; Universitätsstrasse 150,
D-44780 Bochum (Germany)

Supporting information for this article is given via a link at the end of the document.

is in line with previous reports on its mineral crystal structure.[27] While the platelets are comprised of layers of $Fe_{4.5}Ni_{4.5}S_8$ (Figure 1D), such layers are not visible in the hexagonal crystals and no notable surface structuring is observed (Figure 1E). The different morphology can be explained by slightly altered crystal formation processes and an inhomogeneous temperature distribution over the course of the 16 days synthesis.

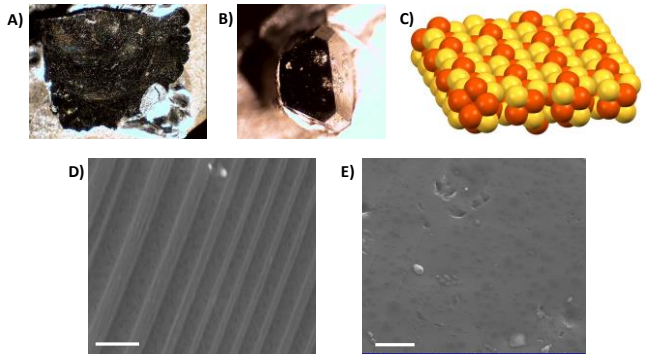

Figure 1. Images of **A)** platelet and **B)** hexagonal shaped $Fe_{4.5}Ni_{4.5}S_8$ crystals. $Fe_{4.5}Ni_{4.5}S_8$ crystal structure with a top view of the (111)-plane **(C)** along with the electron micrographs of the platelet (**D**, scale bar 1 µm) and hexagonal (**E**, scale bar 2 µm) shaped crystals. The nickel and iron sites (orange) are equally distributed within the crystal and are bridged by sulphur (yellow).

After crystal growth, the intrinsic catalytic activity of the crystalline $Fe_{4.5}Ni_{4.5}S_8$ material was evaluated using SECCM (see. Figure 2A for the schematic experimental set-up). By means of SECCM, amperometric or voltammetric measurements were performed in the confined area defined by the meniscus (droplet) cell created between the pulled double-barrel nanopipet probe (SECCM tip; electron micrograph shown in Figure 2A, inset) and substrate (working electrode) surface. Local voltammetric measurements were performed using a previously described "hopping-mode" protocol,[24,28–30] as represented schematically in Figure 2B, in which the SECCM tip was approached to the sample sequentially at a series of predefined locations. Upon each landing of the microdroplet a linear-sweep (LSV) or cyclic voltammogram (CV) was recorded. The geometric area of the electrochemical cell (*i.e.*, the evaluated active catalyst area), defined by the "footprint" of the meniscus (droplet) cell, was readily visualized, post-experiment, using scanning electron microscopy (SEM), as shown in Figure 2C.

A representative LSV measured on a hexagonal-shaped $Fe_{4.5}Ni_{4.5}S_8$ (111) single-crystal basal surface [electron back-scatter diffraction (EBSD) data shown in the Supporting Information, Figure S2] using SECCM is shown in Figure 3A. This LSV, which is the average of 98 individual measurements at different locations, is shifted by *ca.* –60 mV compared to that measured macroscopically of the bulk material (Supporting Information, Figure S3). This is unsurprising, because, as previously alluded to, the macroscopic measurement reveals the "average" properties of all exposed surface sites and features of the bulk material, whereas the SECCM measurement targets a specific surface site, *i.e.*, the (111) crystallographic plane in this case. This indicates that the "enhanced" bulk activity found for the $Fe_{4.5}Ni_{4.5}S_8$ (111) single-crystal surface is likely attributable to the presence of defect sites.

The SECCM meniscus probe was landed on a macroscopic feature ('crack') on the $Fe_{4.5}Ni_{4.5}S_8$ (111) surface (SEM image shown in Figure S4A) in order to simulate a surface "defect" site; a representative LSV is shown in Figure 3A. Clearly, the HER is facilitated at the macroscopic defect site, evident from the *ca.* 4-fold increase in *J* at a given *E* or *ca.* +100 mV shift in the LSV (*i.e.*, compare the pink and blue curves in Figure 3A). We propose that the different reactivity at the defect sites stems from a faster sulfur release rate at such edges, resulting in a faster substitutional protonation and therefore a higher activity, which is in agreement with results recently obtained by operando phonon spectroscopy.[18]

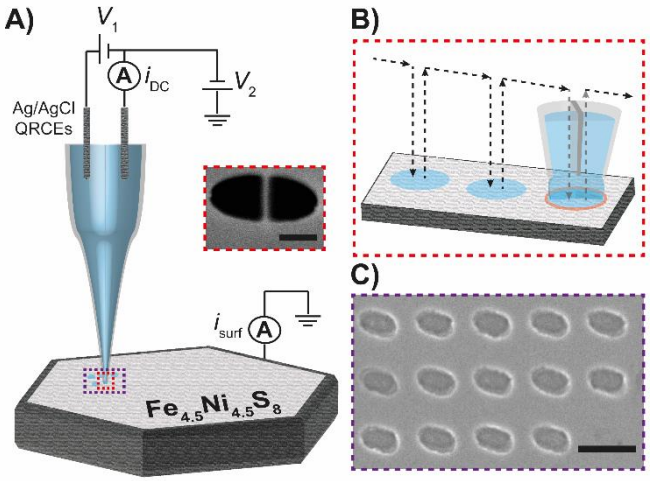

Figure 2. A) Schematic showing the spatially-resolved electrocatalytic measurements obtained using SECCM. A bias voltage (+0.05 V) of V_1 was applied between the two Ag/AgCl wire quasi-reference counter electrodes (QRCEs) and the resulting ion conductance current (i_{DC}) was measured and employed for tip positioning and monitoring the status of the meniscus cell. A voltage of V_2 was applied to one of the QRCEs to control the working electrode (*e.g.*, $Fe_{4.5}Ni_{4.5}S_8$) potential (E_s), where $E_s = -(V_1/2 + V_2)$ and the working electrode current (i_{surf}) was measured. A SEM image of the end of a representative nanopipet probe is shown in the inset (scale bar 200 nm). **B)** Voltammetric hopping-mode SECCM protocol, where the arrows show the movement of the nanopipet probe along the substrate surface. **C)** SEM image of the droplet "footprints" left on the surface of the sample after a cathodic polarization experiment (scale bar 1 µm).

Verifying this behavior on the macroscale would be challenging, necessitating the preparation of samples with engineered surface defects. It should be noted that it is assumed that the presence of the surface defect ("crack") does not significantly influence the probed surface area (*i.e.*, effective electrode area). This is because the dimensions of the feature are relatively minor on the scale of the probed area (Figure S4A) and the fact that the DC and AC ion conductance currents (i_{DC} *and* i_{AC}, induced by V_1 in Figure 2A), which indicate on the morphology of the meniscus cell, do not vary significantly from that measured on the [111] basal surface (Supporting Information, Figure S4B to E). In addition, as mass transport (*i.e.*, proton diffusion) would be expected to be greatly hindered within the confined dimensions of the *ca.* 40 nm wide "crack", the effective electrode area (caused by electrolyte "wicking" into the crack) would need to increase by more than a factor of 4 to explain the enhanced currents in Figure 3A. Given that droplet spreading on the basal surface is minimal (*i.e.*, the dimensions of the droplet footprints are comparable to the tip

diameter, see Figure 1), such an increase in the effective surface area is very unlikely and thus the enhanced *J* in Figure 3A is attributed to a legitimate increase in activity (HER kinetics), as discussed above.

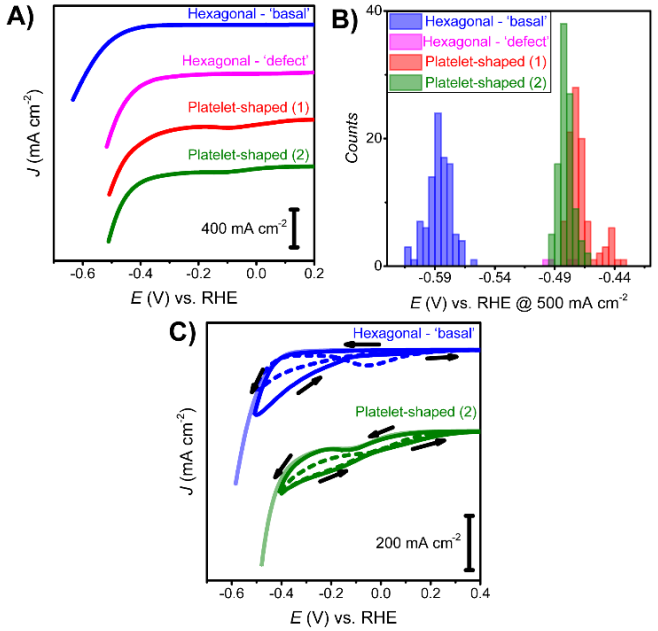

Figure 3. A) Averaged LSVs (scan rate, v = 250 mV s^{-1}, $[HClO_4]$ = 0.1 M) obtained from a hexagonal $Fe_{4.5}Ni_{4.5}S_8$ (111) crystal basal surface (blue trace) and macroscopic defect site ('crack', pink trace) and; Fe-rich areas of platelet-shaped crystals (red and green traces). B) Histograms showing the distribution in E at a J of 500 mA cm^{-2}. The number of measurements (N) in **A)** and **B)** were 98, 4, 97 and 101 for the blue, pink, red and green traces, respectively. **C)** Averaged CVs (v = 250 mV s^{-1}, $[HClO_4]$ = 0.1 M) obtained from hexagonal $Fe_{4.5}Ni_{4.5}S_8$(111) (N = 240, blue trace) and an Fe-rich area of a platelet-shaped crystal (N = 297, green trace). The first and second cycles are indicated by solid and dashed lines, respectively. The arrows indicate the direction of the first sweep. Note that the probed surface area (effective electrode area) was assumed to be unperturbed by the presence of the macroscopic defect (crack).

The enhanced activity at the macroscopic defect site on $Fe_{4.5}Ni_{4.5}S_8$ (111) is also clearly evident in Figure 3B, which shows the distribution in potential at a current density J of 500 mA cm^{-2}. Mean values of –0.59 V (N = 98) and –0.48 V (N = 4) were derived for the $Fe_{4.5}Ni_{4.5}S_8$ (111) basal surface and macroscopic defect site, respectively. These microscopic data indicate that defect-rich $Fe_{4.5}Ni_{4.5}S_8$ (111) would be more active than the pristine bulk material. It is worth noting that the values measured at the $Fe_{4.5}Ni_{4.5}S_8$ (111) basal surface follow a normal distribution, with a standard deviation of 0.01 V. This clearly demonstrates the reproducibility of the SECCM technique for performing nanoscopic electrocatalytic measurements at single-crystal surfaces, which allows tens to hundreds of spatially-resolved LSVs to be recorded in different areas of a surface in a matter of minutes.[8,24]

Additional platelet-shaped crystalline $Fe_{4.5}Ni_{4.5}S_8$ samples were also evaluated using the SECCM technique; representative LSVs are shown in Figure 3A. Evidently, the two samples possess enhanced HER activity, with the LSVs (*i.e.*, red and green traces) each being shifted by *ca.* +100 mV compared to the hexagonal $Fe_{4.5}Ni_{4.5}S_8$ (111) crystal basal surface discussed above (*i.e.*, blue trace). In addition, there is a clear difference at the foot of the LSV, which was further investigated by cyclic voltammetry with SECCM, as shown in Figure 3C. While the $Fe_{4.5}Ni_{4.5}S_8$ (111) hexagonal crystal gives rise to a relatively featureless CV, with a positive hysteresis on the reverse sweep, there is a prominent shoulder in the CV of the "high activity" platelet-shaped sample. These differences suggest that there are either different crystallographic orientations exposed or there is a difference in the atomic composition of the sample surfaces. The former was ruled out by EBSD analysis and the latter was confirmed by energy-dispersive X-ray spectroscopy (EDX; Supporting Information, Figure S5). While most spots investigated on the sample surfaces possess the expected Fe : Ni : S ratio as in the original material (*e.g.*, Fe : Ni : S; 1 : 1.1 : 1.8; Figure S5A), the "high activity" regions show a significantly altered atomic composition. These regions instead are Fe-rich and reveal a relatively lowered S-content [Fe : Ni : S; 1 : 0.4 : 1.4 and 1 : 0.4 : 1.3 for (1) and (2), Figure S5B and C] and are most-likely a result of the long-thermal treatment during the preparation of the material.

It was previously noted that pentlandite-like compounds containing different Fe : Ni ratios exhibit similar surface compositions; a mixture of iron and nickel sulfides as well as Fe^{3+} oxidic species and $Ni(OH)_2$, as revealed by XPS. No clear influence on the HER activity was, however, observed for the as prepared samples.[31] It should also be noted that, as shown earlier by operando phonon studies on $Fe_{4.5}Ni_{4.5}S_8$, activation processes correlated with S-depletion and formation of defect sites were found to dramatically increase the HER activity of the pentlandite, consistent with what has been observed here (Figure 3A).[16,18,31]

Returning to Figure 3B, platelet samples (1) and (2) possess mean potential values at 500 mA cm^{-2} of –0.47 ± 0.01 V (N = 97) and -0.48 ± 0.01 V (N = 101), respectively. It is also interesting to note that in the Fe-rich area of platelet sample (1), there are clearly two populations present in the distribution exhibiting substantially different potentials at 500 mA cm^{-2} values; a large one (N = 83) centered around –0.47 V and a much smaller one (N = 14) centered around –0.44 V. Again, the "higher activity" population is supposed to arise from surface defect sites exposed on the $Fe_{4.5}Ni_{4.5}S_8$ crystal surface, which, as noted above is suggested to give rise to more rapid sulfur release/protonation rates and thus enhanced HER catalytic activity.

The prominent reductive shoulder observed for the "high activity" platelet samples, prior to the HER wave (as seen in Figures 3A and C) arises from a change in the material itself (*i.e.*, "aging"). A somewhat smaller reduction process ("shoulder") prior to the HER wave is also observed at the hexagonal $Fe_{4.5}Ni_{4.5}S_8$ bulk surface during the second voltammetric cycle (dashed trace, Figure 3C), consistent with macroscopic measurements performed using the bulk material (see Figure S3). The larger pre-wave (shoulder) currents associated with the Fe-rich "high activity" areas are indicative of a faster "aging" ("corrosion") process compared to the $Fe_{4.5}Ni_{4.5}S_8$ basal surface. If this "aging" stems from sulfur release and substitutional protonation, as alluded to above, this may explain the increased activity in these samples. DFT calculations of defect-free and S vacancy- containing $Fe_{4.5}Ni_{4.5}S_8$ (111) structures indicate preferential substitutional adsorption of H atoms at different vacancies within the crystal lattice. The influence of the vacancies position on the energy threshold of the process was previously discussed in detail.[18] These theoretical calculations

were supported by experimental nuclear resonant inelastic X-Ray scattering, both highlighting the importance of defects for the increased HER activity. Furthermore, this observation suggests that Fe-rich areas are less stable due to increased susceptibility to corrosion and thus might lead to higher HER activity on the experimental (*i.e.*, s to min) timescale due to a facilitation of the substitutional sulfur/hydrogen replacement.

In conclusion, we have utilized SECCM to unveil the structural and compositional controls on electrocatalytic activity for iron nickel sulfide, $Fe_{4.5}Ni_{4.5}S_8$. Small variations in the surface Fe : Ni : S ratio, achieved through varying synthesis conditions or material "aging", can lead to a tremendously altered catalytic HER activity. In a more general sense, this study demonstrates how information on surface structure and atomic composition within an investigated (nano)material can be directly correlated to spatially-resolved electrochemical information, which is a crucial step in rational catalyst design and synthesis. In this regard, SECCM could have an important role in resolving structure-activity relationships in complex electrocatalytically active materials and in heterogeneous catalyst discovery.

Acknowledgements

C.L.B. acknowledges support from a Marie Curie Individual Fellowship (702048 NEIL). P.R.U. thanks the Royal Society for a Wolfson Research Merit Award. U.-P.A. is grateful for the financial support by the Fonds of the Chemical Industry (Liebig grant) and the Deutsche Forschungsgemeinschaft (Emmy Noether grant to U.-P.A., AP242/2-1 and AP242/6-1). W.S. is grateful for financial support from the Deutsche Forschungsgemeinschaft in the framework of the cluster of excellence "RESOLV" (EXC1069). The authors thank Mr. Lewis Yule and Dr. Geoff West for performing EBSD.

Keywords: electrocatalysis; iron-nickel-sulfide; SECCM; hydrogen evolution reaction; single-crystal surface

[1] Z. W. Seh, J. Kibsgaard, C. F. Dickens, I. Chorkendorff, J. K. Nørskov, T. F. Jaramillo, *Science* **2017**, *355*, DOI 10.1126/science.aad4998.
[2] W. Lubitz, W. Tumas, *Chem. Rev.* **2007**, *107*, 3900–3903.
[3] J. M. Ogden, *Phys. Today* **2002**, *55*, 69.
[4] G. W. Crabtree, M. S. Dresselhaus, M. V. Buchanan, *Phys. Today* **2004**, *57*, 39–44.
[5] X. Zou, Y. Zhang, *Chem. Soc. Rev.* **2015**, *44*, 5148–5180.
[6] "ExxonMobil's 2017 Outlook for Energy PDF reports," can be found under http://corporate.exxonmobil.com/en/energy/energy-outlook/download-the-report/download-the-outlook-for-energy-reports, **2017**.
[7] W. Sheng, Z. Zhuang, M. Gao, J. Zheng, J. G. Chen, Y. Yan, *Nat. Commun.* **2015**, *6*, DOI 10.1038/ncomms6848.
[8] C. L. Bentley, M. Kang, F. M. Maddar, F. Li, M. Walker, J. Zhang, P. R. Unwin, *Chem. Sci.* **2017**, *8*, 6583–6593.
[9] D. Merki, X. Hu, *Energy Environ. Sci.* **2011**, *4*, 3878–3888.
[10] J. Kibsgaard, Z. Chen, B. N. Reinecke, T. F. Jaramillo, *Nat Mater* **2012**, *11*, 963–969.
[11] B. Konkena, J. Masa, W. Xia, M. Muhler, W. Schuhmann, *Nano Energy* **2016**, *29*, 46–53.
[12] M. A. Lukowski, A. S. Daniel, F. Meng, A. Forticaux, L. Li, S. Jin, *J. Am. Chem. Soc.* **2013**, *135*, 10274–10277.
[13] Z. Lei, S. Xu, P. Wu, *Phys Chem Chem Phys* **2016**, *18*, 70–74.
[14] J. D. Benck, T. R. Hellstern, J. Kibsgaard, P. Chakthranont, T. F. Jaramillo, *ACS Catal.* **2014**, *4*, 3957–3971.
[15] B. Hinnemann, P. G. Moses, J. Bonde, K. P. Jørgensen, J. H. Nielsen, S. Horch, I. Chorkendorff, J. K. Nørskov, *J. Am. Chem. Soc.* **2005**, *127*, 5308–5309.
[16] B. Konkena, K. junge Puring, I. Sinev, S. Piontek, O. Khavryuchenko, J. P. Dürholt, R. Schmid, H. Tüysüz, M. Muhler, W. Schuhmann, et al., *Nat. Commun.* **2016**, *7*, 12269–12277.
[17] K. junge Puring, S. Piontek, M. Smialkowski, J. Burfeind, S. Kaluza, C. Doetsch, U.-P. Apfel, *J. Vis. Exp.* **2017**, *124*, DOI 10.3791/56087.
[18] I. Zegkinoglou, A. Zendegani, I. Sinev, S. Kunze, H. Mistry, H. S. Jeon, J. Zhao, M. Y. Hu, E. E. Alp, S. Piontek, et al., *J. Am. Chem. Soc.* **2017**, 14360–14363.
[19] G. Zhang, P. M. Kirkman, A. N. Patel, A. S. Cuharuc, K. McKelvey, P. R. Unwin, *J. Am. Chem. Soc.* **2014**, *136*, 11444–11451.
[20] C.-H. Chen, K. E. Meadows, A. Cuharuc, S. C. S. Lai, P. R. Unwin, *Phys. Chem. Chem. Phys.* **2014**, *16*, 18545–18552.
[21] P. R. Unwin, A. G. Güell, G. Zhang, *Acc. Chem. Res.* **2016**, *49*, 2041–2048.
[22] N. Ebejer, A. G. Güell, S. C. S. Lai, K. McKelvey, M. E. Snowden, P. R. Unwin, *Annu. Rev. Anal. Chem.* **2013**, *6*, 329–351.
[23] R. G. Mariano, K. McKelvey, H. S. White, M. W. Kanan, *Science* **2017**, *358*, 1187–1192.
[24] C. L. Bentley, M. Kang, P. R. Unwin, *J. Am. Chem. Soc.* **2017**, *139*, 16813–16821.
[25] T. F. Jaramillo, K. P. Jørgensen, J. Bonde, J. H. Nielsen, S. Horch, I. Chorkendorff, *Science* **2007**, *317*, 100–102.
[26] Y. Li, H. Wang, L. Xie, Y. Liang, G. Hong, H. Dai, *J. Am. Chem. Soc.* **2011**, *133*, 7296–7299.
[27] A. Pearson, M. Buerger, *Am. Mineral.* **1956**, *41*, 804–805.
[28] S. P. E, Y.-R. Kim, D. Perry, C. L. Bentley, P. R. Unwin, *ACS Appl. Mater. Interfaces* **2016**, *8*, 30458–30466.
[29] C.-H. Chen, L. Jacobse, K. McKelvey, S. C. S. Lai, M. T. M. Koper, P. R. Unwin, *Anal. Chem.* **2015**, *87*, 5782–5789.
[30] A. G. Güell, A. S. Cuharuc, Y.-R. Kim, G. Zhang, S. Tan, N. Ebejer, P. R. Unwin, *ACS Nano* **2015**, *9*, 3558–3571.
[31] S. Piontek, C. Andronescu, A. Zaichenko, B. Konkena, K. junge Puring, B. Marler, H. Antoni, I. Sinev, M. Muhler, D. Mollenhauer, et al., *ACS Catal.* **2018**, 987–996.

COMMUNICATION

Local investigation of the hydrogen evolution reaction (HER) on single crystal iron nickel sulphide, one of the most active non-noble metal based HER catalyst, was carried out using Scanning Electrochemical Cell Microscopy (SECCM). Small variations in the Ni:Fe ratio at the surface induce tremendous changes in the catalytic HER activity.

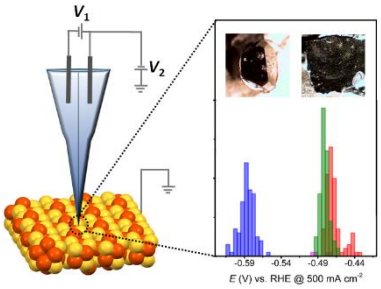

Cameron L. Bentley, Corina Andronescu, Mathias Smialkowski, Minkyung Kang, Tsvetan Tarnev, Bernd Marler, Patrick R. Unwin, Ulf -Peter Apfel,* Wolfgang Schuhmann**

Page No. – Page No.

Local surface structure and composition control the hydrogen evolution reaction on iron nickel sulfides